Journal of Photochemistry & Photobiology, A: Chemistry 424 (2022) 113629

Contents lists available at ScienceDirect

Journal of Photochemistry & Photobiology, A: Chemistry

journal homepage: www.elsevier.com/locate/jphotochem

Visible light-driven photocatalyst: An iron(III) coordination compound in Rhodamine B degradation

Esmeralda Ortiz-Zarco [a,b], Dora Solis-Casados [c], Luis Escobar-Alarcón [d], Ivan García-Orozco [b,*]

[a] Universidad Autónoma del Estado de México, Facultad de Química, Programa de Maestría en Ciencias Químicas, Paseo Colón esq. Paseo Tollocan s/n, Toluca, México CP 50120, Mexico

[b] Universidad Autónoma del Estado de México, Facultad de Química. Laboratorio de Investigación y Desarrollo de Materiales Avanzados (LIDMA), Carretera Toluca-Atlacomulco Km 14.5, Unidad San Cayetano, Toluca, México CP 50100, Mexico

[c] Universidad Autónoma del Estado de México, Facultad de Química, Centro Conjunto de Investigación en Química Sustentable UAEM-UNAM, Carretera Toluca-Atlacomulco Km 14.5, Unidad San Cayetano, Toluca, México CP 50100, Mexico

[d] Departamento de Física, Instituto Nacional de Investigaciones Nucleares, Carretera México-Toluca S/N, La, Marquesa, CP 52750 Ocoyoacac, Estado de México, Mexico

ARTICLE INFO

Keywords:
Iron complexes
Photocatalytic degradation
Rhodamine B
Scavenger
Kinetic rate constants

ABSTRACT

Rhodamine B (RhB) was photocatalytically degraded by an iron(III) complex (FeL_3, L = Methyl 3-hydroxy-2-propenedithioate). The photocatalysts were synthesized, supported on glass slides, and characterized by elemental analyses, IR, UV–vis, Raman, TGA, XPS, Diffuse Reflectance spectroscopy, and Powder X-ray diffraction analyses. The iron complex was also impregnated onto titania (TiO_2) films to enhance the photocatalytic performance of this oxide. The structure of the complex does not change when supported on a glass substrate. The FeL_3 showed a band gap value (E_g = 1.32 eV) lower than TiO_2 (Eg = 3.38 eV), whereas the FeL_3 sensitized titania showed the highest E_g value (Eg = 3.41 eV). The photocatalytic degradation of RhB by the TiO_2-FeL_3 system (27%) after 180 min of reaction slightly improves the performance of TiO_2 (22%). Remarkably, FeL_3 film showed the best performance (34%). When using scavengers, the degradation reveals that the produced superoxide radicals seem to be responsible for the RhB degradation.

1. Introduction

Photocatalysis can degrade organic compounds into smaller molecules (bleaching), or ever CO_2 and water (mineralization) in an environmentally friendly way to become one of the most beneficial wastewater treatments. Several photocatalysts have been proved, being the TiO_2 in its anatase phase, one of the most active photocatalysts. However, this titania phase is photoactive only under UV irradiation due to its high band gap energy close to 3.2 eV [1]. Therefore, it is of great interest to investigate photocatalysts susceptible to be excited under visible light, which intend to photodegrade organic pollutants.

One of the molecular approaches towards a visible-light-driven photocatalyst is the use of transition metal complexes. In general, ruthenium, osmium, and iridium complexes have been extensively studied as sensitizers [2]. It has been reported that iron compounds act as visible lighted photocatalysts with additional advantages such as being the least toxic and least expensive materials [3]. The photocatalysts iron complexes have been used in three key areas: (a) in the preparation of necessary chemical compounds, (b) as a photoinitiator in polymer synthesis, and (c) in the degradation of harmful or undesirable compounds. Degradation reactions using iron complexes as photocatalyst were applied in model molecules for wastewater treatments, as organic contaminants (phenol [4], 4-chlorophenol [5], 4-chlorophenolacetic acid [6], dimethylaniline [7], or oxalates [8]), drugs (norfloxacin [4], gemfibrozil [9], naproxen [9], hydrochlorothiazide [9], chloramphenicol [10], diclofenac [11], or 2,4-xilidine [12]), or dyes (Rhodamine B [13,7], orange II [14], methyl orange [13], or malachite green [7]).

Rhodamine B (RhB) is one of the most common dyes used in paints, textiles, paper, among other things. This molecule fluoresces and is used as a tracer in biotechnology, microscopy, and other spectroscopy applications [15]. However, the RhB is chemically stable and with low biodegradability producing water pollution. We are interested in the iron(III) complexes derived from a β-oxodithioesther ligand as a

* Corresponding author.
E-mail address: igarciao@uaemex.mx (I. García-Orozco).

https://doi.org/10.1016/j.jphotochem.2021.113629
Received 19 May 2021; Received in revised form 29 September 2021; Accepted 24 October 2021
Available online 30 October 2021

photocatalyst. To our best knowledge, there are only five reports on Rhodamine B photodegradation by iron complexes [7,13,14,16,17]. Three catalysts are iron complex over different inorganic supports (laponite or amberlite) to avoid iron leaching. It is important to note that iron(II) complexes have higher degradation times (up to 100 h [7]) than the iron(III) complexes (between 15 min [13] to 3 h [14]). All of them reach the total degradation of RhB using H_2O_2, except $[Fe(bpy_3)]^{2+}$-amberlite, but extent the reaction time to completely degrade the dye. However, the mineralization reached by the particular system is only 60%, evidencing a blanching not mineralization of these photocatalytic systems [7,17]. The ligands of the iron complexes are N- or O-donors, and in only one instance, there is an SCN ligand coordinating to the iron center [16].

This work describes the photocatalytic evaluation of the [tris-(Methyl 3-hydroxy-3-phenyl-2-propenedithioate)iron(III)] complex (FeL_3) in the Rhodamine B degradation, an iron(III) sulfur-coordinated complex. The findings reveal the excellent photocatalytic performance of the FeL_3 complex in contrast with the Titania thin films. Likewise, it was noticed that the impregnation of titania with FeL_3 slightly improves its photocatalytic performance. Additionally, the reaction path of the degradation process was evaluated by the photocatalytic reactions in the presence of scavenger-type molecules.

2. Experimental

2.1. Material and methods

Titanium isopropoxide (Sigma-Aldrich), dichloromethane, ethanol, hexane, isopropyl alcohol, sodium sulfate, sodium hydroxide, nitric acid, and $FeCl_3{\cdot}6H_2O$ (Fermont) were used without previous purification. The ligand methyl 3-hydroxy-3-phenyl-2-propenedithioate (L) was prepared using a methodology developed by our group [18]. A solution of 10 μmol/L of Rhodamine B dye (Sigma-Aldrich, $C_{28}H_{31}ClN_2O_3$), which has a characteristic absorption band peaking at 526 nm, was used as a model molecule representative of an organic pollutant. Standard microscope glass slides (Velab, México) were used as substrates. The 26 × 26 × 1 mm glass slides were first cleaned with detergent and washed with distilled water. Afterward, they were rinsed with acetone, ethanol, and distilled water and dried at 70 °C for 15 min.

2.2. Preparation of the complex [tris-(methyl 3-hydroxy-3-phenyl-2-propenedithioate-S,O)-iron(III)] [FeL_3]

Sodium hydroxide (0.9 ml, 1.2 M) was added to methyl 3-hydroxy-3-phenyl-2-propenedithioate ligand (0.3 g, 1.43 mmol) in ethanol (25 ml). A water solution of iron(III) chloride (0.1286 g, 0.476 mmol) was added to the mixture under stirring. The reaction was extracted with dichloromethane, the organic phase was dried over sodium sulfate, and the solvent was evaporated under reduced pressure. The resulting dark green solid was washed with hexane and dried under a vacuum. Yield 0.118 g (36%), Mp: 224 °C dec. Anal. Calcd. for $C_{30}H_{27}FeO_3S_6$ (683.91): C 52.69, H 3.98. Found: C 52.20, H 4.24.

2.3. Preparation of the TiO_2 thin film

TiO_2 thin films were obtained by spin coating using as a precursor the sol prepared with titanium isopropoxide (1.86 g, 6.553 mmol) in 10 ml of 2-propanol under vigorous stirring for 30 min. Nitric acid (1 ml, 70%) was added drop by drop, keeping the stirring 30 min more. The jellified precursor was deposited layer to layer over a glass slide using a KW-4A Chemat Technology Spin Coater at 1800 rpm for 30 s repeating this procedure 15 times. The deposited titania precursor was dried at room temperature all night and then was annealed at 400 °C for 3 h to obtain the anatase phase.

2.4. Characterization of the thin films

Infrared spectra were acquired on a Bruker Tensor 27 with an ATR diamond MIRacle-Reflection accessory with a resolution of 8 cm^{-1} and 32 scans. Elemental analyses were performed on an Elementar Vario MICRO cube equipment. XPS spectrum was obtained on a JEOL JPS-9200 with an X-ray source of Mg (1253.6 eV) at 200 W, 1 mm analysis area, and 10^{-8} Torr. The spectrum was analyzed with specsurf™ software included in the instrument. The carbon signal (C1s) at 284.5 eV corrects the charge of the data. The spectrum fitting uses Shirley's method for the noise extraction and Gauss-Lorentz curves. The films were characterized by Raman and diffuse reflectance spectroscopies. Raman spectra were acquired using an HR LabRam 800 system equipped with an Olympus BX-40 confocal microscope; an Nd: YAG laser beam (532 nm) was focused by a 100x objective onto the sample surface, with a spectral resolution of 2 cm^{-1}, and 16 scans. Diffuse Reflectance Spectroscopy (DRS) measurements were carried out with a Perkin Elmer Lambda 35 spectrophotometer equipped with an integrating sphere. The band gap energy (E_g) was estimated using the Kubelka-Munk function. The powder X-ray diffraction analyses were carried out in a Bruker D8 Advance diffractometer with a detector Linxeye, using the Cu-K_α radiation ($\lambda = 1.541$ Å), 30 kV and 30 mA of tube potency, a spectral window 2θ from 5 to 50°, step size 0.1°, and step time 1 s.

Particles in suspension have positive and negative charges in equilibrium at a specific pH value. This fact is a characteristic of the material and correlates with the isoelectric point (IEP). The value determines the ability to adsorb cations or anions, which depends on the pH of the impregnating solution. The FeL_3 IEP was determined with a Zeta-meter system 3.0. 25 mg of FeL_3 complex was dissolved with 3 ml of LiCl 0.1 M and adjusted to 250 ml. The pH was adjusted with LiOH and HCl, and the dissolution was sonicated to disperse the suspended solids. An aliquot was placed in the zeta-meter and 100 mV of potential was applied. The charge potential of the particles is plotted as a function of pH value.

2.5. Photocatalytic experiments

The photocatalytic performance of the films was evaluated in the Rhodamine B (RhB) degradation. For this purpose, the catalyst film was immersed in 20 ml of the dye solution (10 μmol/L), keeping it in the dark up to reach the adsorption equilibrium (30 min). Then the system was illuminated by a solar simulator (SF-150B class ABA from ScienceTech) with a 2″ diameter spot size at one sun emitting 6% of UV radiation. The light source was placed 15 cm above the surface of the solution. The reaction was followed by the RhB characteristic absorption band at λ = 526 nm, correlated with RhB concentration by a calibration curve. The data were fitted onto a non-linear pseudo-first-order kinetic model to determine the rate constant of the photocatalytic process (κ_{app}). Half-life ($t_{1/2}$) was obtained by the k_{app} constant using the equation: $t_{1/2} = 0.693/k_{app}$. The Total Organic Carbon (TOC) was determined by the combustion method, for each solution, as carbon ppm. The mineralization degree of the RhB solution is obtained by quantifying the initial (TOC_0) and final (TOC_f) total organic carbon of photolysis, TiO_2, and FeL_3, following the next equation: mineralization (%) = $[1 - (TOC_f/TOC_0)] \times 100$.

2.6. Photocatalytic reactions using Scavenger-type molecules.

Additionally, to gain insight into the degradation reaction route, photocatalytic experiments with scavenger-type molecules were performed. Triethanolamine (TEOA, 0.01 M), *p*-benzoquinone (BZQ, 0.001 M), and isopropanol (IPA, 0.02 M) were employed as scavengers for photogenerated holes (h^+), superoxide anion radicals ($O_2^{-\cdot}$) and hydroxyl radicals (OH•) [19], respectively. For this purpose, the radical scavengers (TEOA 10 mM, BZQ 1 mM, or IPA 20 mM) were placed into the dye solution before the irradiation. Degradation of RhB was followed

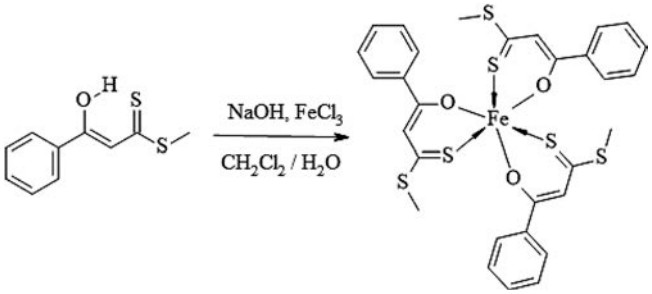

Scheme 1. Preparation of the FeL_3 complex from the ligand Methyl 3-phenyl-3-hydroxy-2-propenedithioate.

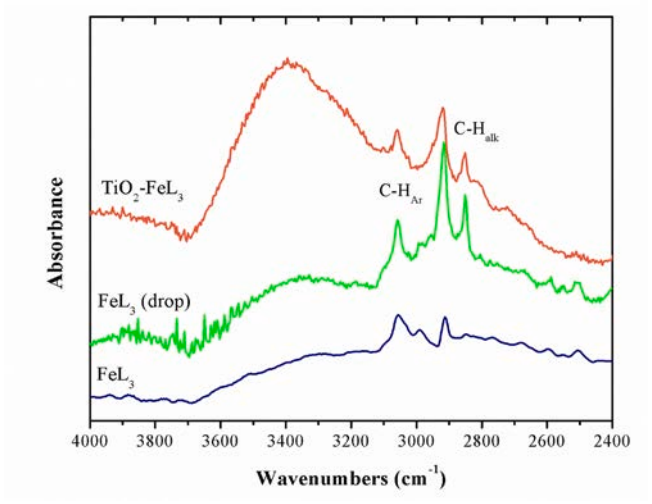

Fig. 1. IR spectra from 4000 to 2400 cm^{-1} of the complex in powder (FeL_3), supported on a glass substrate (FeL_3 (drop)) and impregnated on Titania (TiO_2/FeL_3).

by the process described above.

3. Results and discussion

3.1. 1 Preparation of the iron complex FeL_3

The iron complex FeL_3 was obtained by the straightforward reaction of the sodium ligand salt in ethanol and an aqueous iron(III) chloride solution (Scheme 1). The elemental analyses (Experimental section) give insights above the composition of the complex, proving the presence of the three ligand molecules by one iron atom. The color was the first indicator of the FeL_3 existence: a yellowish solution changed to a dark green mixture. The iron complex was extracted with dichloromethane in quantity yields. Once the solvent of the organic phase was evaporated, a greenish-black solid was obtained. The complex in the solid phase was more stable than in the dichloromethane solution. The latter is degraded slowly to a yellowish suspension. The complex is soluble only in dichloromethane or chloroform and is insoluble in the rest of the common solvents, water included. This fact is crucial since the complex is not soluble in the reaction medium, and therefore the photocatalytic reaction is carried out heterogeneously.

3.2. Spectroscopic and structural evidence of the FeL_3 formation

The structure of iron complex FeL_3 was elucidated by certain spectroscopic techniques. The IR and Raman spectra give evidence of the coordination mode of the ligand. TGA shows the thermal stability of the complex and the loss of ligands fragments that confirm the presence of three ligands around the metal ion. XPS analyses provide information on the iron oxidation state and verify the coordination of the metal to oxygen and sulfurs donor atoms. The DRS spectra evidence the electronic transitions that occurred in the complex. The XRD diffractogram shows the crystalline nature of the complex and displays a new solid phase than those reported for other iron(III) complexes. The following sections will describe in detail each characterization.

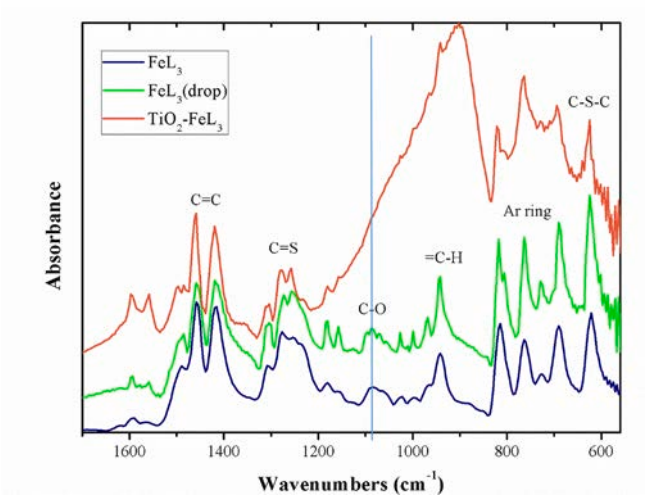

Fig. 2. IR spectra from 1700 to 550 cm^{-1} of the complex as powder form (FeL_3), supported on a glass substrate (FeL_3 (drop)), and impregnated on titania (FeL_3/TiO_2).

3.2.1. IR analyses of FeL_3 complex

The IR spectra were acquired in two regions of interest, from 4000 to 2400 cm^{-1} (Fig. 1) and from 1700 to 550 cm^{-1} (Fig. 2). The complex structure is evidenced by the characteristic bands observed in the IR spectrum (FeL_3 in Figs. 1 and 2). The signals at 621 and 1240 cm^{-1} were assigned to C-S-C and C = S vibration modes of the dithioester group [20]. The ligand carbon structure is evidenced by the bands at 3055, 2912 (C–H vibration), 690, and 763 (out-of-plane C–H bending vibration for a monosubstituted aromatic ring) [21], and 814 cm^{-1} related to the ring deformation of the in-plane bending vibration [22]. The band at 941 cm^{-1} can be assigned to the = C–H group [23] and besides the signal at 1058 cm^{-1} (C-O vibration) confirm the enol moiety. This band is shifted 22 cm^{-1} towards low wavenumbers respecting the ligand (at 1080 cm^{-1}) due to the coordination to the iron center. The C-O vibration decreases its energy (and consequently its bond order) due to the electron donation of the oxygen atom to the iron ion. The band assigned to the C = S vibration at 1240 cm^{-1} is shifted 40 cm^{-1} to lower wavenumbers (1280 cm^{-1} in the ligand), reducing its bond order due to the electron donation of the sulfur atom to the iron atom. This wavenumber shifts evidence of the coordination mode of the β-oxo-dithioester toward the iron ion by sulfur and oxygen donor atoms as a chelate.

3.2.2. Raman analyses of FeL_3 complex

The assignation of the Raman spectra (FeL_3 in Fig. 3) has been made using the IR spectra. Both IR and Raman spectra are linked by symmetry. The Raman analyses were acquired from 50 to 1100 cm^{-1} since in this range main vibrational features appears. The Raman signals of the FeL_3 complex in powder are observed at 944 (=C–H vinyl), 825, 706 (out of plane deformation signals of phenyl ring), 632 (C-S-C vibration), 524, 354 (Fe-O bond) [24], and 310 cm^{-1} (Fe-S bond) [25] (Fig. 3). These bands confirm the assignation made by IR spectroscopy and provide more insights into the coordination mode of the ligand.

3.2.3. TGA analysis of FeL_3 complex

The thermogram of the FeL3 complex shows that the compound is

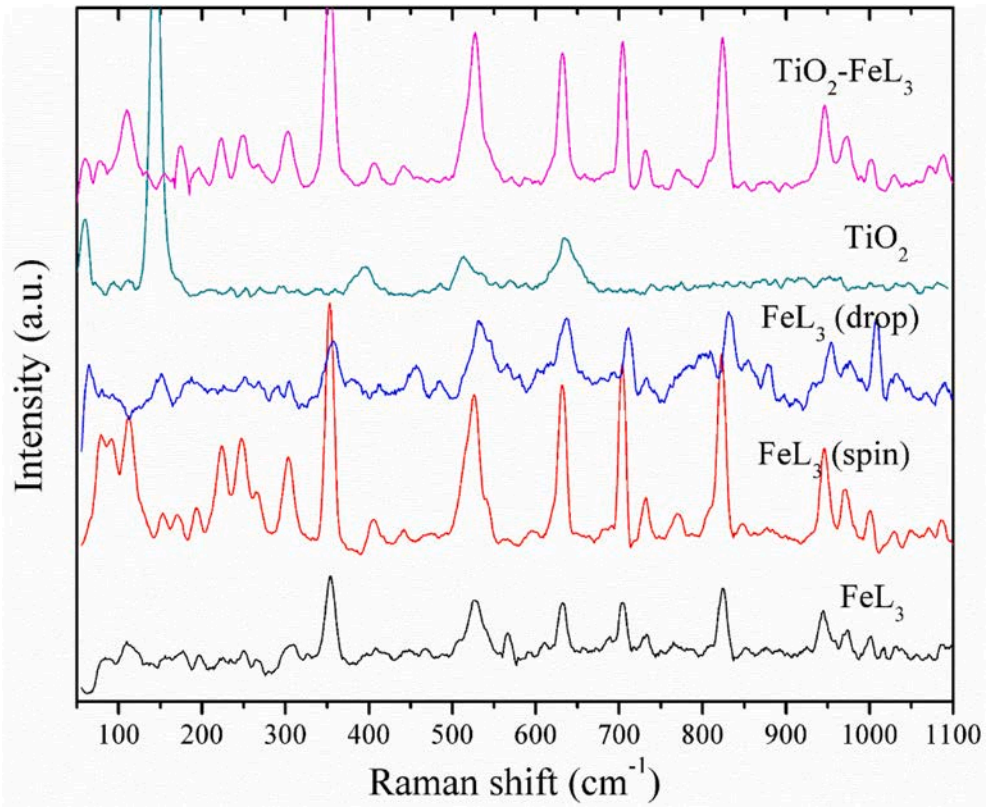

Fig. 3. Raman spectra of the complex in powder (FeL_3), deposited on a glass substrate by spin coating (FeL_3 (spin)), dropping a dichloromethane solution (FeL_3 (drop)), a Titania thin film (TiO_2) and the Titania film impregnated with the iron complex (TiO_2-FeL_3).

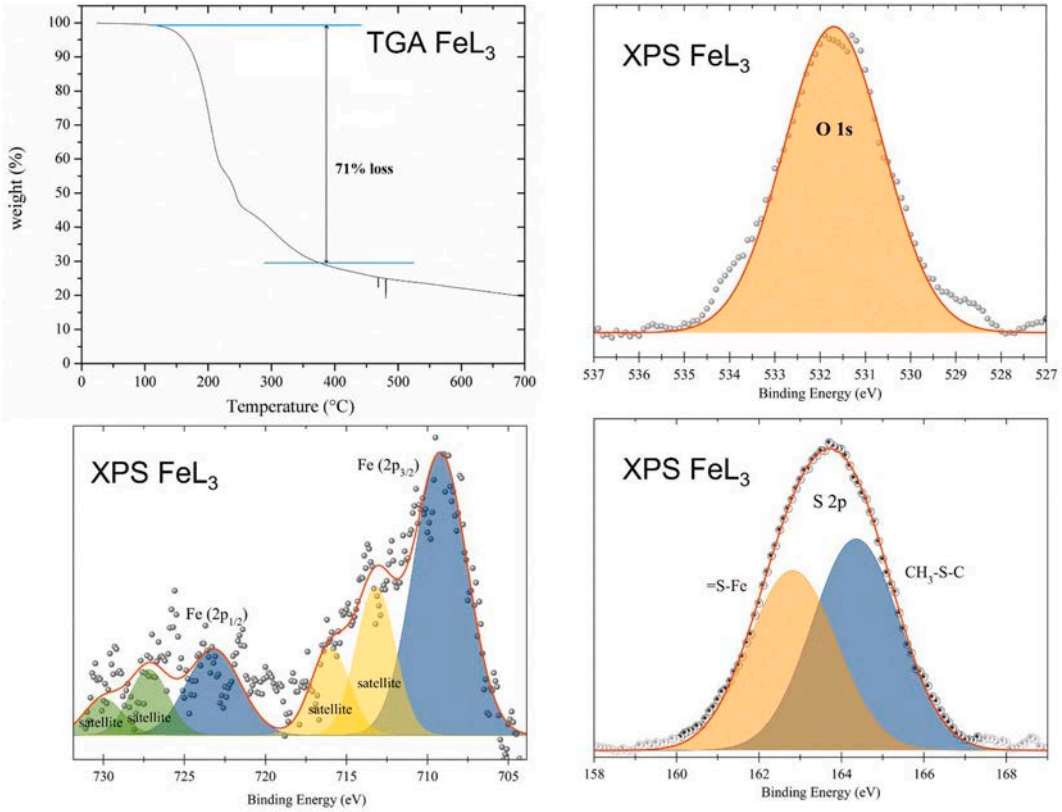

Fig. 4. TGA thermogram and XPS spectra of the complex FeL_3.

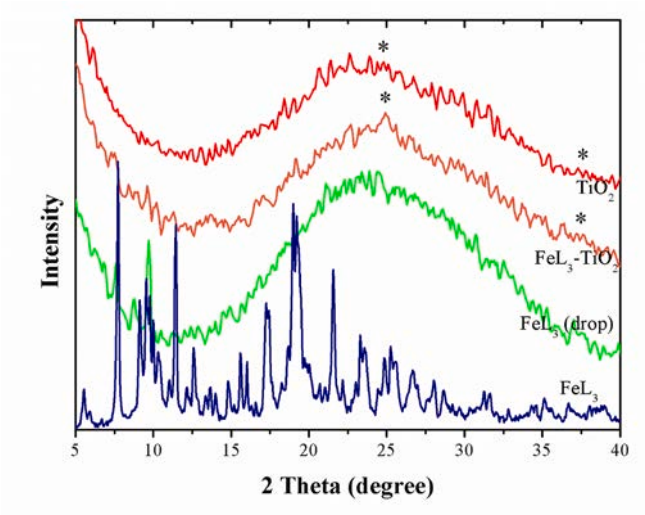

Fig. 5. X-ray diffraction patterns of the complex in powder (FeL_3), supported on a glass substrate (FeL_3 (drop)), and Titania impregnated (TiO_2/FeL_3), compared with the Anatase phase (*).

thermal stable up to 100 °C. Before that temperature, the complex has a 71% loss of weight up to 385 °C. The inorganic residue could be matching the formula FeO_3S_3 (200 g/mol), which could be related to the 29 % weight. In this sense, the initial mass should be quoted as 689 g/mol, similar to the calculated molar mass of the complex (683.9 g/mol), considering three ligands in the structure. In the case of a complex formula of FeL_2, the residue will have a mass of 152 g/mol (the same 29%w), and the overall initial weight should be 524 g/mol, more than the expected 474 g/mol, corresponding to the theoretical mass of FeL_2 complex.

3.2.4. *XPS analyses of FeL_3 complex*

The XPS spectra of the complex are shown in Fig. 4. The binding energies of Fe ($2P_{1/2}$) and Fe ($2P_{3/2}$) electrons (respectively at 723.2 and 709.2, FWHM = 3.9) correspond to an octahedral iron(III) center similar to those previously described [27]. The Fe 2P spectrum displays two satellite signals at higher energies for both peaks, separated by 4 and 6.8 eV from the mainline. The satellites could be interpreted as paramagnetism at the metal center. The O (1S) spectrum shows one peak at 531.7 eV (FWHM = 2.6 eV), similar to some [Fe(acac)$_3$] reported [26,27]. The S (2P) spectrum shows two peaks at binding energies of 162.8 and 164.4 eV with FWHM = 2.5 eV. The difference in BE (1.6 eV) is larger than the doublet splitting reported for S (2P) signals (between 1.0 and 1.2 eV), then each peak corresponds to different species. The peak at 164.4 eV was assigned to the -SMe moiety and, the peak at 162.8 eV corresponds to the C = S group coordinated to the iron center. When a dithiocarboxylate moiety is present in the molecule structure, the S (2P) binding energy is around 164 eV [28,29]. The coordination of the sulfur atom decreases the BE in 1.4–1.6 eV respecting the BE associated with the non-coordinated sulfur atom [28]. Furthermore, the -SMe component is more intense than the C = S-Fe component, as stated by Chehimi and Delamar [29], confirming the assignation. In summary, the XPS analyses show an iron(III) center coordinated by an Oxygen atom and by the C = S group of the ligand molecule, supporting the observed in the IR analyses.

3.2.5. *XRD analyses of FeL_3 complex*

The XRD pattern of the powder FeL_3 complex is displayed in Fig. 5. The powder complex FeL_3 shows a crystalline appearance that could generate an adequate monocrystal for its monocrystal XRD diffraction study. Further crystallization experiments are in the course to obtain the right sample to determine its crystalline structure. However, to the aim of this work, the peaks observed in the powder XRD pattern are only reported. The FeL_3 complex shows peaks at 2θ values of 7.7°, 9.1°, 9.6°, 9.8°, 10.0°, 10.3°, 11.4°, 12.6°, 14.8°, 15.6°, 16.3°, 17.2°, 18.6°, 19.0°, 19.2°, 20.0°, 21.6°, 23.3°, 23.6°, 24.9°, 25.3°, 25.5°, 26.7°, 28.0°, 28.6°, 31.3°, 31.6°, 34.3°, 35.1°, and 36.7°, being the most intense those at 2-theta = 7.7°, 9.6°, 11.4°, 17.2°, 18.6°, and 21.6°. These peaks do not correspond with any reported iron(III) compound pattern, therefore, up to our best knowledge this is the first time that the XRD pattern of the FeL_3 complex is reported.

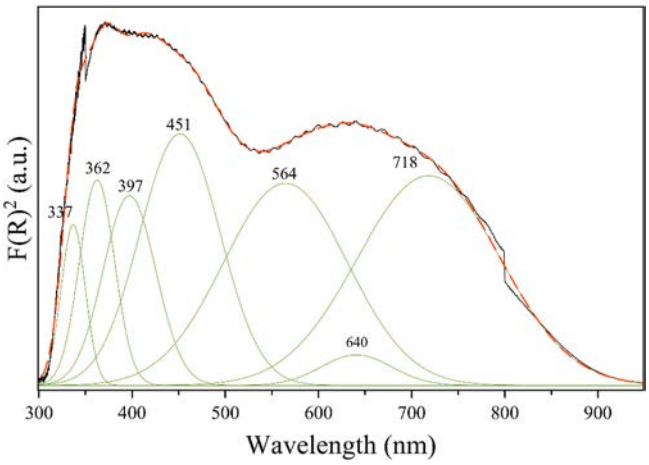

Fig. 6. UV–vis absorption spectrum for FeL_3 complex, deconvoluted for its better assignation.

3.2.6. *UV–vis analyses of FeL_3 complex*

The UV–vis absorption spectrum of the FeL_3 complex in powder form shows strong absorption bands in the ultraviolet and visible regions (Fig. 6). For a better analysis, the absorption spectrum was deconvoluted using gaussian functions. The bands centered at 337, 362, and 397 nm were assigned to the electronic transitions of the ligand (Ligand Centered, LC), specifically to the aromatic K-band, α, β-unsaturated system K-band, and n → π* transitions of C = S moiety, respectively [30]. The band at 451 nm was assigned to metal to ligand charge transfer band (MLCT), commonly observed in iron(III) complexes [31–33]. The bands above 500 nm were assigned to metal d-d transitions (Metal Centered, MC). The six-coordinate iron(III) presents $^6A_{1g}\rightarrow{}^4T_{1g}$, $^6A_{1g}\rightarrow{}^4T_{2g}$, and $^6A_{1g}\rightarrow{}^4T_{1g}$ transitions, which were associated with the bands at 564, 640, and 718 nm, respectively [34].

3.3. *The FeL_3 supporting over glass or titania.*

It was needed to deposit the iron coordination compound on a glass substrate for its application as a photocatalyst. In that way, it is avoided the solid–liquid separation stage allowing easy removal from the photodegradation reaction system [7,16,17]. The deposition of the complex on the substrate was carried out by drop-casting and spin-coating techniques. These deposits were used to evaluate their performance in the RhB photodegradation. In general terms, some drops of a dichloromethane solution of the complex (2 mM) were deposited on the glass substrate layer by layer, up to get to five layers, allowing to dry between each layer.

On the other hand, since the FeL_3 compound has a deep dark green color owing to the metal to ligand charge transfer band (MLCT), it could act as a titania sensitizer [35]. To prove this, one milliliter of the complex solution (2 mM) was deposited on a titania film, drying it at room temperature. The aim was to study how the FeL_3 complex affects the photocatalyst performance of the titania film.

The vibrational features of the complex FeL_3 do not shift when supported on the substrates (glass or titania). Notably, the drop-casting

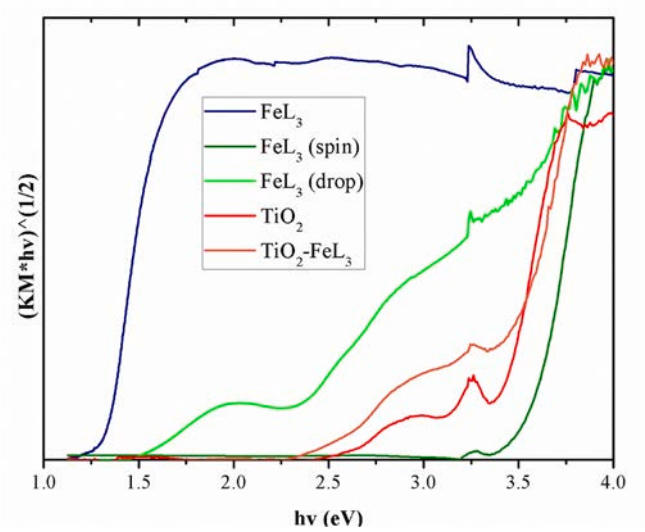

Fig. 7. Tauc plots of the powder complex (FeL_3) supported in a glass substrate by spin coating (FeL_3 (spin)), dropping a dichloromethane solution (FeL_3 (drop)), and Titania impregnated (TiO_2-FeL_3), respecting to the Titania thin film (TiO_2).

process produces more defined signals in IR spectra by solvent evaporation, inducing a better crystal orientation than those observed in powder. Figs. 1 and 2 show the IR spectra of the complex supported on a glass substrate (FeL_3 (drop)) and Titania (TiO_2-FeL_3). The IR bands at 621, 690, and 763, 814, 941, 1058, and 1240 cm^{-1} evidence the presence of the complex. The broad bands centered around 3400 (Fig. 1), 900, and 700 cm^{-1} (Fig. 2) on the IR spectrum of TiO_2-FeL_3 correspond to the Titania structure [36]. All other bands associated with the complex are similar to the FeL_3 and FeL_3 (drop) samples. The complex structure does not change when it is impregnated in the Titania film. Notwithstanding the broadband centered at 3400 cm^{-1} is commonly associated with O–H groups as water molecules (Fig. 1), the band at 1640 cm^{-1} is missing (Fig. 2), suggesting no water molecules over the film surface.

In general, the Raman spectra of the FeL_3 complex (Fig. 3) in different forms show the same main features with minor differences. The FeL_3 sample deposited by spin coating shows more intense peaks than the others. The Raman spectrum of the Titania film shows peaks at 143, 399, 517, and 638 cm^{-1} (Fig. 3) associated with the TiO_2 anatase phase of [37]. The TiO_2-FeL_3 Raman spectrum predominantly shows the FeL_3 peaks, similar to the FeL_3 (spin) spectrum. The signal in 180 cm^{-1} could be related to the most intense signal of the Anatase phase at 144 cm^{-1}, shifted by the impregnation. The Titania film is covered with the FeL_3 complex, disappearing in the Raman spectrum.

The XRD diffractograms of TiO_2, FeL_3 (drop), and TiO_2.FeL_3 samples show a broad band centered at 2-theta = 25 due to the glass substrate utilizing as support. The sample peaks are partially covered under this amorphous phase that is why some minor intensity peaks might be assigned. In the case of the FeL_3 (drop), the peaks observed at 2θ values of 7.6°, 8.8°, 9.7°, and 21.0° suggest the presence of the FeL_3 complex. These peaks could be related to a preferred orientation of the FeL_3 when is deposited over the glass substrate. The representative peaks of the Titania are not observed in the TiO_2 nor in TiO_2.FeL_3 because the film has a small amount to make the diffraction analysis. The diffractogram of TiO_2.FeL_3 shows some broad and weak peaks at 25.0° and 36.3°, assigned to the Anatase phase (JCPD 84–1286). In this sample can also be observed weak signals at 7.5°, 9.6°, 11.3°, 17.1°, and 19.2° associated with the presence of the FeL_3 complex.

The supported FeL_3 complex does not change its structure with the deposition process. It is important to note that the preparation process affects the amount of FeL_3 complex over the surface. The spin-coating could produce an apparent more homogeneous film over the substrate but with a minimal amount of the complex: the solution is wasting with the coating process. However, it could seem that the orientation of the complex is better than the drop-casting methodology, as seen in Raman spectra of the FeL_3 (spin) sample.

Table 1
Bandgap values Eg (eV) for the photocatalyst used.

Compound	E_g (eV)	Transition
FeL_3	1.32	Allowed indirect
FeL_3 (spin)	3.54	Forbidden indirect
FeL_3 (drop)	2.18	Allowed indirect
TiO_2	3.38	Allowed indirect
TiO_2-FeL_3	3.41	Allowed direct

3.4. The band gap of the supported FeL_3 complex

Fig. 7 shows the Tauc plots for the different samples. The profile of the Tauc plot varies notably for each photocatalyst (Fig. 6). The FeL_3 complex displays an absorption edge in the near-infrared region (below 1.5 eV). On the other side, TiO_2, TiO_2-FeL_3, and FeL_3 (spin) samples show the absorption edge in the UV region (up to 3.1 eV). Only the FeL_3 (drop) shows an absorption edge in the visible region (from 1.5 to 3.1 eV). It is important to note that the compacted powder of the FeL_3 complex has a lower energy absorption edge when it is on the glass support. This change could be due to a greater surface area and hence a better absorption of light. The absorption edge of the FeL_3 (spin) sample is similar to the glass support, then the amount of complex supported is insufficient to quantify the absorption. This fact is more evident at viewing the supporting materials (spin and drop) because the color is more pronounced with a large amount of the complex, up to a greenish-black solid of the powder complex. The increase of the complex amount produces significant light absorption.

The band gaps (E_g) were calculated by the Tauc plots and are summarized in Table 1. The E_g value for Titania (3.38 eV) is similar to those values previously reported [37]. The E_g values of the samples evidence their semiconductor nature and display the following order: FeL_3 < FeL_3 (drop) < TiO_2 < TiO_2.FeL_3 < FeL_3 (spin). It is important to note that the FeL_3 E_g is an infrared region activated. However, the support of FeL_3 over a glass substrate shifts the band gap toward lower energy up to the visible region. The E_g value is similar to those reported for iron complexes among 2.0 to 2.8 eV [38,39,35]. The TiO_2-FeL_3 E_g is similar to TiO_2 suggesting that the titania band gap is not affected by the FeL_3 impregnation.

3.5. Isoelectric point

The isoelectric point (IEP) was determined for the FeL_3 complex. The pH where there are positive and negative charges in equilibrium is the isoelectric zero charge point. In this case, the FeL_3 complex has a value of IEP = 6.5. This value indicates that under pH < 6.5, the FeL_3 particles are positively charged, and the interaction with anions is easier. Above this pH value, the FeL_3 are negatively charged, and the anions interact more easily with the surface. The RhB has a cationic structure, therefore at pH > 6.5 is favored its interaction with the negatively charged surface of the supported FeL_3 complex. This fact favors the agglomeration of RhB molecules over the FeL_3 surface make it more available for the photodegradation process.

3.6. Catalytic performance of photocatalysts FeL_3

The catalytic performance was studied by following the degradation of a Rhodamine B (RhB) solution (10 μmol/l) as a function of the irradiation time. The degradation degree of RhB for all the catalysts is depicted in Fig. 8. The reaction degradation was followed by UV–vis

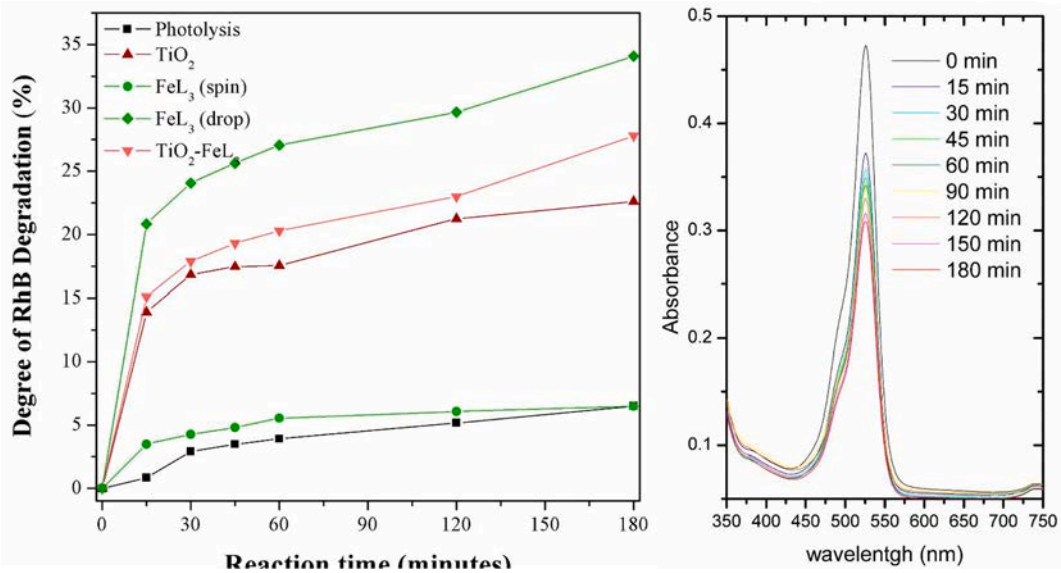

Fig. 8. Photocatalytic degradation of Rhodamine B (RhB) using FeL_3, TiO_2, and TiO_2-FeL_3 films, and photolysis (left). UV–vis spectra of the RhB degradation versus time, for FeL_3 (drop) photocatalysis (right).

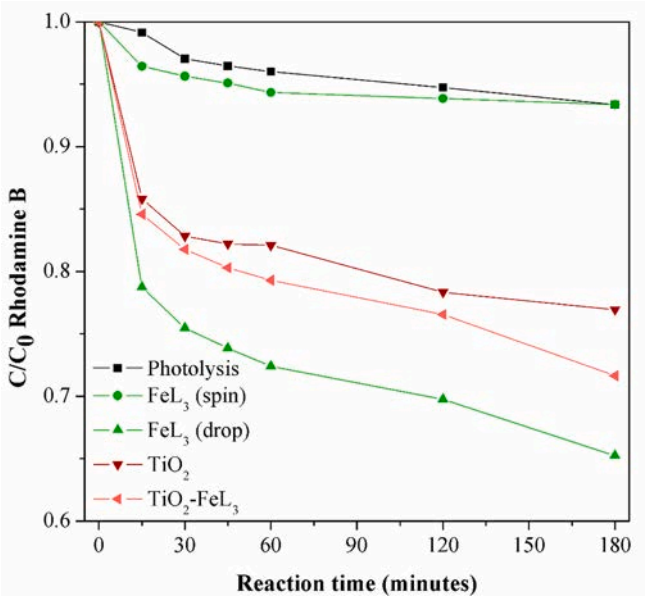

Fig. 9. The (C/C_0) values versus the reaction time of all the films evaluated in the Rhodamine degradation by visible light.

spectroscopy, and it is noteworthy that RhB disappears after illumination, and no other products could be identified in the reaction media by UV–vis spectroscopy (Fig. 8, right).

The uncatalyzed process (photolysis) achieves only 6.5% of degradation after 180 min of reaction. The catalyzed process using the Titania film as a photocatalyst reaches 22.6% of RhB degradation at the same time. The FeL_3 samples show a different catalytic performance depending on the preparation technique. The catalyzed process using the FeL_3 film prepared by dropping a dichloromethane solution of the iron complex reaches 34.1% of degradation. On the other hand, the catalyzed process using the FeL_3 (spin) reaches only 7.4% of RhB degradation, close to those achieved by the uncatalyzed process. This low activity is probably due to the low amount of iron complex deposited over the glass substrate. When the Titania impregnated by the FeL_3 complex is used as a catalyst, the RhB degradation reaches 27% after 180 min of reaction. The TiO_2-FeL_3 performance is 5% better than the TiO_2 film. This fact indicates that the FeL_3 complex slightly improves the catalytic behavior of Titania.

Table 2
Kinetic parameters: constant rates k_{app} (min^{-1}) and $t_{1/2}$ (min) for prepared photocatalysts, and the scavengers study.

Process catalyzed or uncatalyzed	k_{app} (10^{-2} min^{-1})			$t_{1/2}$ (min)		
	un-scav.	IPA	TEOA	un-scav.	IPA	TEOA
Photolysis	1.6 ± 0.4	5.2 ± 1.1	3.6 ± 0.5	44.5	13.4	19.5
FeL_3 spin	4.0 ± 0.9	*nd*	*nd*	17.5	*nd*	*nd*
FeL_3 drop	10.5 ± 0.9	3.9 ± 2.0	1.1 ± 0.3	4.5	17.7	63.8
TiO_2	5.8 ± 0.9	0.2 ± 0.2	1.6 ± 0.2	11.8	293.7	44.5
TiO_2-FeL_3	6.9 ± 1.1	6.3 ± 0.9	4.1 ± 0.6	10.1	11.0	16.8

nd: not determined.

The photocatalysis causes the mineralization of RhB as determined by the mineralization degree. For the photolysis and TiO_2 photocatalysis, the mineralization reaches 10 and 27%, respectively, at 180 min of reaction. While for FeL_3 photocatalysis, the mineralization achieves a 29% at the same time. The degradation percent and the mineralization have similar values (6.5, 22.6, and 34.1%, for photolysis, TiO_2, and FeL_3, respectively), then the RhB photodegradation achieves the mineralization of the compound. The FeL_3 complex prepared by drop-casting can perform an efficient RhB photodegradation.

To estimate the reaction rate, the kinetic analysis of RhB degradation was performed from the plot of the (C/C_0) values versus the reaction time (Fig. 9). The reaction rate values were adjusted using a pseudo-first-order expression applying the least-squares method [40]. Table 2 shows the Kinetic rate constant (k_{app}) in min^{-1} and half-life time ($t_{1/2}$) in min for all catalysts studied.

The photoactivity begins before 15 min of lighting, as can be seen in Fig. 9. In general, the (C/C_0) values versus the reaction time plots do not fit a linear model. If the photolysis curve is adjusted with a linear correlation, the correlation coefficient is $R^2 = 0.8716$, and the rest of the photocatalysts correlate with $R^2 < 0.7$ or less. Therefore, there were

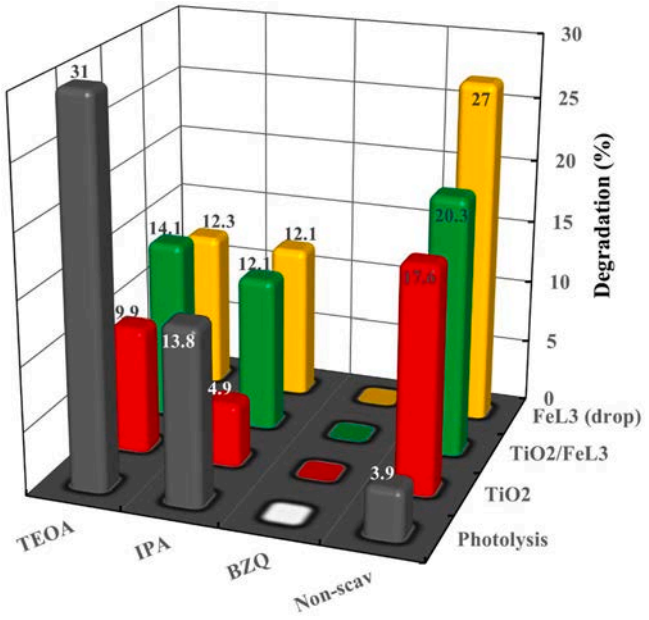

Fig. 10. Photodegradation in the presence of scavengers after 60 min of reaction time.

necessary to adjust with a more complex model. The curves better fit a pseudo-first-order expression with an $R^2 > 0.95$ in all the cases. The kinetic parameters are resumed in Table 2. The photolysis and FeL_3 (spin) films show an apparent similar performance (Fig. 8), but comparing their constant rates, the degradation with FeL_3 (spin) is 2.5 times faster than photolysis (by the ratio of FeL_3 (spin) / photolysis constant rates). The RhB degradation is accelerated by the presence of the FeL_3 complex, despite its supported low amount. Similarly, the FeL_3 (drop) is 2.8 faster than the spin coating preparation. The low amount of the complex and the distribution over the substrate could be associated with this behavior. It is important to note that the constant rate of FeL_3 (drop) is higher than those reported for other iron complexes in RhB degradation (0.105 min^{-1}). The UV light-driven photodegradation systems have lower values than those visible activated (0.0147 min^{-1} for a TiO_2/GO/hemin catalyst [41] against 0.0285 min^{-1} for a $[Fe(bpy)_3]$/laponite system [17]), using H_2O_2 as the oxidant for RhB degradation. But in all instances, k_{app} has a smaller value than FeL_3 (drop) system. Moreover, the system $[Fe(bpy)_3]$/amberlite[7] does not use H_2O_2 as oxidant and has the lowest values than our catalyst (6.3×10^{-8} min^{-1}), evidencing a slow degradation process in similar RhB concentration and reaction conditions.

The RhB photodegradation using TiO_2 as a catalyst shows a logarithm behavior before to 60 min. After this time displays a linear model. This fact evidences a possible change in the mechanism of photodegradation, about 60 min. In this case, the dye degradation is 3.6 faster than photolysis. The TiO_2.FeL_3 catalyst improves the reaction rate by 19%, which indicates an electronic interaction between TiO_2 and FeL_3.

3.7. The photodegradation mechanism of FeL_3

The absorption of a photon with energy equal to or greater than the bandgap of the photocatalyst promotes an electron from the valence band to the conduction band, creating a hole in the valence band. If the generated photocharges reach the photocatalyst surface, they can produce hydroxyl (OH·) and superoxide radicals (O_2^-), respectively, when interacting with oxygen or water molecules. The role of these species in the photodegradation mechanisms was investigated by reactive species trapping experiments using different scavengers [42–44]. The addition of Triethanolamine (TEOA), p-benzoquinone (BZQ), and isopropanol (IPA) to the reactions system were employed to impede the reaction of

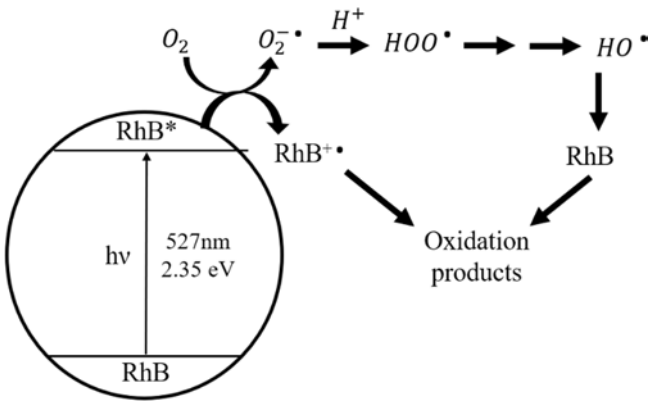

Fig. 11. The RhB photolysis mechanism.

RhB molecules with holes (h^+), superoxide anion (O_2^-), and hydroxyl radicals ($HO^·$), respectively [19,45]. Figs. 10 and 11 show the photodegradation with TiO_2, FeL_3 (drop), and TiO_2.FeL_3 samples, using the different scavenger molecules, and Table 2 summarizes the kinetic parameters of the reactions using these molecules.

The use of scavenger-type molecules in the photodegradation of RhB allows determining the reaction path favored by each photocatalyst. The RhB photodegradation is inhibited by benzoquinone (BZQ) in all cases, indicating that superoxide radicals play a relevant role in the reaction. Such a result, the created photoelectrons are the responsible species to produce the catalytic activity. It is important to note that the photolysis reaction increases from 3.9 to 13.8% of RhB degradation with the blocking of the hydroxyl radicals by isopropanol (IPA). Therefore, the hydroxyl radicals role does not seem to be relevant in the performance of the tested photocatalysts. Triethanolamine (TEOA) increases the photolysis about eight times, respecting the non-scavenger process (from 3.9 to 31% of RhB degradation). These facts agree with the dye photolysis mechanism shown in Fig. 10 [46]. The $\lambda = 527$ nm photon absorption produces an excited state of the molecule of Rhodamine (RhB*). Afterward, this excited molecule interacts with an oxygen molecule to form the superoxide radical anion and $RhB^{+\cdot}$ which decompose to oxidation products. When the BZQ suppresses the superoxide radical anion formation, the RhB degradation stops. The IPA reduces the hydroxyl radicals and thus decreases the superoxide radical anion decomposition, increasing the RhB degradation. Furthermore, TEOA probably interacts with the $RhB^{+\cdot}$ enhancing its degradation to a great extent.

The photocatalytic process has multiple contributions to molecular degradation activity. The catalyzed photodegradation is produced by holes (h^+), hydroxyl radicals ($HO^·$), and superoxide radicals ($O_2^{-\cdot}$) [47], as evidenced by the addition of scavenger-type molecules (IPA, BZQ, and TEOA). The previous results showed that the addition of BZQ inhibits the RhB photodegradation. On the other side, the created photoelectrons interact with oxygen molecules producing superoxide radicals which have great importance in the RhB degradation. The photodegradation is not entirely stopped with IPA or TEOA addition. Only a decrease in the activity compared to the process without scavengers was observed.

In the case of titania, the BZQ completely inhibits the RhB photodegradation provoked by the superoxide radical. The same result is observed with the IPA addition. The photodegradation decreases by 76%, respecting the non-scavenged process (from 17.9 to 4.3 degradation %). In this case, the hydroxyl radical plays a significant role in RhB degradation, similar to the superoxide radical. However, TEOA decreases RhB degradation by 56%, respecting the non-scavenged process (from 17.9 to 10.1%). These results reveal that the holes (h^+) do not have a significant role in the RhB degradation, whereas the $HO^·$ and $O_2^{-\cdot}$ radicals are more relevant in the RhB oxidation.

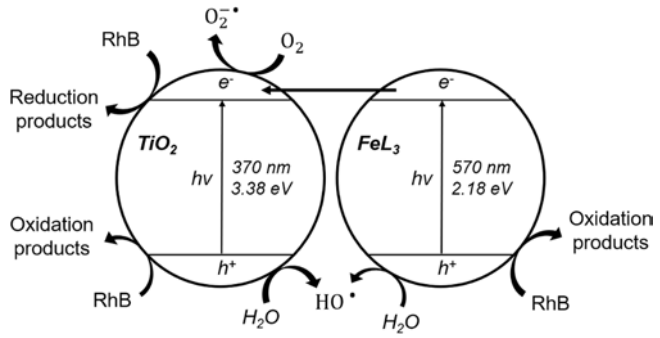

Fig. 12. The RhB photocatalysis mechanism by TiO_2-FeL_3 system.

The photocatalysis with the iron complex is slightly different than in the case of titania. In this instance, IPA and TEOA inhibit about 55% of the RhB degradation, respecting the process without scavengers (12.1% for IPA and 12.3% for TEOA, considering 27.1 degradation %). RhB degradation by the iron complex is influenced by the following order: $O_2^{-\cdot} > h^+ \approx HO^\cdot$. The sensitization of titania (TiO_2-FeL_3) seems to improve the photocatalytic performance. The combination of the iron complex with titania causes a minor deactivation of the active sites. In this sense, IPA and TEOA inhibit 40 and 30% of the RhB degradation, respectively (12.1 and 14.2 degradation %, against 20.3% reached without scavengers). The proposed mechanism with the TiO_2/FeL_3 photocatalyst is depicted in Fig. 12.

The behavior of C/Co versus irradiation time (Fig. 13) shows an increment of the relative concentration (C/Co) when using BZQ as an inhibitor. This fact may be attributed to an interaction between RhB and BZQ without degradation of the dye [19]. In the photolysis of RhB, the degradation increases with the presence of TEOA (ca. 10%) and IPA (ca. 30%) regarding the process without scavengers.

For photolysis, the rate constants for TEOA and IPA increase respecting the photodegradation without scavengers (225% for TEOA and 325% for IPA, Table 2). RhB photodegradation becomes more efficient when the formation of $RhB^{+\cdot}$ is promoted. On the other side, photocatalytic degradation becomes slower with IPA and TEOA than reactions without scavengers. The mechanism is different than photolysis. For TiO_2, the rate constant decreases 97% with IPA and 72% with TEOA, evidencing the significant role of $HO^\cdot$ radicals and the holes (h^+) in the photodegradation. The case for FeL_3 (drop) is different. In general, the FeL_3 (drop) is almost twice as fast as TiO_2 for reactions without scavengers. Therefore, there will be greater photodegradation. The rate constant of FeL_3 (drop) decreases 63% for IPA and 89% for TEOA. The holes (h^+) play a more significant role in the photodegradation than the hydroxyl radical. When FeL_3 sensitizes TiO_2, the reactive species changes respecting TiO_2. The rate constant of TiO_2-FeL_3 decreases slightly for IPA (9%) and 41% for TEOA. In this case, the hydroxyl radical becomes less crucial in the photodegradation respecting holes (h^+). In summary, photocatalytic degradation of RhB is controlled by more than one active species, in the following order: $O_2^{-\cdot} > HO^\cdot > h^+$.

4. Conclusions

The [tris-(Methyl 3-hydroxy-3-phenyl-2-propenedithioate)iron(III)] complex (FeL_3) was obtained as a solid product. The ligand is O, S-coordinated to the iron(III) ion in a chelated form. The FeL_3 complex structure does not change when it is supported on a glass slide. In this case, the electronic transitions of the complexes decrease their intensity. The band gap of the powder FeL_3 is in the infrared region (1.32 eV), but when it is on a glass substrate, the band gap is shifted to the visible

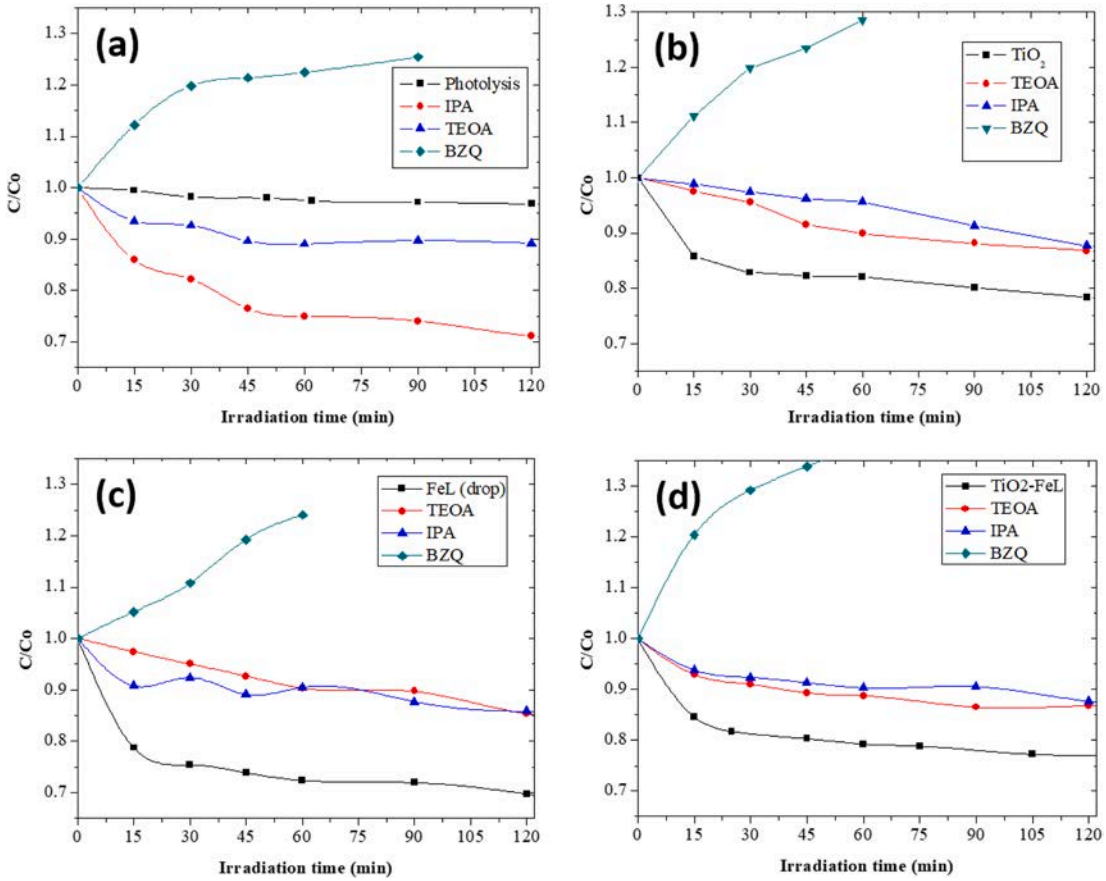

Fig. 13. Effect of different scavengers on the RhB photodegradation by (a) Photolysis, (b) TiO_2, (c) FeL_3 (drop), (d) TiO_2/FeL_3.

region (2.18 eV). The FeL_3 complex has been successfully employed to photodegraded Rhodamine B without adding hydrogen peroxide in the presence of visible light. The constant rate of FeL_3 (drop) is higher than those reported for other iron complexes in RhB degradation (0.105 min^{-1}). The RhB degradation follows the order: photolysis < TiO_2 < FeL_3 (drop). Furthermore, the sensitization of the titania by the FeL_3 complex improves the catalytic performance of TiO_2. Photocatalytic degradation of RhB is controlled by more than one active species. The photodegradation process is mainly driven by superoxide radicals, in the following order: $O_2^{\cdot-} > HO^{\cdot} > h^+$. The hydroxyl radicals and holes (h^+) also have an important role in the process, depending on the catalyst. In general, the influence of active species follows the order: $O_2^{\cdot-} > HO^{\cdot} > h^+$. The new FeL_3 complex is proposed as an efficient photocatalyst in photodegradation reactions and a good sensitizer of TiO_2. Further research about the crystal structure and redox properties of several other FeL_3 complexes is in progress.

CRediT authorship contribution statement

Esmeralda Ortiz-Zarco: Investigation, Validation. **Dora Solis-Casados:** Methodology, Resources, Writing – review & editing. **Luis Escobar-Alarcón:** Formal analysis, Writing – review & editing. **Ivan García-Orozco:** Conceptualization, Formal analysis, Resources, Writing – original draft, Visualization.

Declaration of Competing Interest

The authors declare that they have no known competing financial interests or personal relationships that could have appeared to influence the work reported in this paper.

Acknowledgements

This research was supported by projects SIEA-UAEMex No. 4358/2017CI and SIEA-UAEMex No. 4978/2020CIB. Esmeralda Ortiz-Zarco thanks to CONACYT for scholarship 291025. Authors thank to Lizbeth Triana, Alejandra Nuñez, Uvaldo Hernández, Melina Tapia and Citlalit Martinez (CCIQS) for their technical assistance.

References

[1] Z. Wei, M. Endo, K. Wang, E. Charbit, A. Markowska-Szczupak, B. Ohtani, E. Kowalska, Noble metal-modified octahedral anatase titania particles with enhanced activity for decomposition of chemical and microbiological pollutants, Chem. Eng. J. 318 (2017) 121–134, https://doi.org/10.1016/j.cej.2016.05.138.

[2] J. Twilton, C. Le, P. Zhang, M.H. Shaw, R.W. Evans, D.W.C. MacMillan, The merger of transition metal and photocatalysis, Nat. Rev. Chem. 1 (7) (2017), https://doi.org/10.1038/s41570-017-0052.

[3] R.S. Jack, G.A. Ayoko, M.O. Adebajo, R.L. Frost, A review of iron species for visible-light photocatalytic water purification, Environ. Sci. Pollut. Res. 22 (10) (2015) 7439–7449, https://doi.org/10.1007/s11356-015-4346-5.

[4] X. Wang, Y. Sun, L. Yang, Q. Shang, D. Wang, T. Guo, Y. Guo, Novel photocatalytic system Fe-complex/TiO2 for efficient degradation of phenol and norfloxacin in water, Sci. Total Environ. 656 (2019) 1010–1020, https://doi.org/10.1016/j.scitotenv.2018.11.419.

[5] L. Zhang, Q. Zhai, X. Zhao, X. Min, Q. Zhu, J. Li, Modified wool-iron biopolymer-based complex as an active heterogeneous decontamination photocatalyst, J. Energy Chem. 25 (6) (2016) 1064–1069, https://doi.org/10.1016/j.jechem.2016.10.010.

[6] K. Lang, S. Luňák, Photocatalytic degradation of 4-chlorophenoxyacetic acid in the presence of an iron complex and hydrogen peroxide, Photochem. Photobiol. Sci. 1 (8) (2002) 588–591, https://doi.org/10.1039/B203147G.

[7] J. Li, W. Ma, Y. Huang, X. Tao, J. Zhao, Y. Xu, Oxidative degradation of organic pollutants utilizing molecular oxygen and visible light over a supported catalyst of Fe(Bpy)32+ in water, Appl. Catal. B Environ. 48 (1) (2004) 17–24, https://doi.org/10.1016/j.apcatb.2003.09.003.

[8] A. Bozzi, T. Yuranova, J. Mielczarski, J. Kiwi, Evidence for immobilized photo-Fenton degradation of organic compounds on structured silica surfaces involving Fe recycling, New J. Chem. 28 (4) (2004) 519–526, https://doi.org/10.1039/B316027K.

[9] V.A.B. Paiva, C.E.S. Paniagua, I.A. Ricardo, B.R. Gonçalves, S.P. Martins, D. Daniel, A.E.H. Machado, A.G. Trovó, Simultaneous degradation of pharmaceuticals by classic and modified photo-Fenton process, J. Environ. Chem. Eng. 6 (1) (2018) 1086–1092, https://doi.org/10.1016/j.jece.2018.01.013.

[10] I. Amildon Ricardo, V.A.B. Paiva, C.E.S. Paniagua, A.G. Trovó, Chloramphenicol photo-fenton degradation and toxicity changes in both surface water and a tertiary effluent from a municipal wastewater treatment plant at near-neutral conditions, Chem. Eng. J. 347 (2018) 763–770, https://doi.org/10.1016/j.cej.2018.04.169.

[11] A.G. Trovó, R.F.P. Nogueira, Diclofenac abatement using modified solar photo-fenton process with ammonium iron(III) citrate, J. Braz. Chem. Soc. 22 (6) (2011) 1033–1039, https://doi.org/10.1590/S0103-50532011000600005.

[12] S.H. Bossmann, N. Shahin, H.L. Thanh, A. Bonfill, M. Wörner, A.M. Braun, [FeII (Bpy)3]2+/TiO2-codoped zeolites: synthesis, characterization, and first application in photocatalysis, ChemPhysChem 3 (5) (2002) 401–407, https://doi.org/10.1002/1439-7641(20020517)3:5<401::AID-CPHC401>3.0.CO;2-7.

[13] J.-W. Ran, S.-W. Liu, P. Wu, J. Pei, Efficient photocatalytic properties of a dinuclear iron complex with bis[2-hydroxybenzaldehyde]hydrazonate ligand, Chin. Chem. Lett. 24 (5) (2013) 373–375, https://doi.org/10.1016/j.cclet.2013.03.015.

[14] H. Ji, W. Song, C. Chen, H. Yuan, W. Ma, J. Zhao, Anchored oxygen-donor coordination to iron for photodegradation of organic pollutants, Environ. Sci. Technol. 41 (14) (2007) 5103–5107, https://doi.org/10.1021/es070021u.

[15] R.F. Kubin, A.N. Fletcher, Fluorescence quantum yields of some rhodamine dyes, J. Lumin. 27 (4) (1982) 455–462, https://doi.org/10.1016/0022-2313(82)90045-X.

[16] S. Lodha, A. Jain, P.B. Punjabi, A novel route for waste water treatment: photocatalytic degradation of rhodamine B, Arab. J. Chem. 4 (4) (2011) 383–387, https://doi.org/10.1016/j.arabjc.2010.07.008.

[17] M. Cheng, W. Ma, C. Chen, J. Yao, J. Zhao, Photocatalytic degradation of organic pollutants catalyzed by layered iron(II) bipyridine complex-clay hybrid under visible irradiation, Appl. Catal. B Environ. 65 (3) (2006) 217–226, https://doi.org/10.1016/j.apcatb.2006.01.010.

[18] M.D.C. Mancilla-González, V. Jancik, D. Martínez-Otero, M. Moya-Cabrera, I. García-Orozco, Half-sandwich titanium complexes with β-oxodithioester ligands, J. Organomet. Chem. 770 (2014) 35–41, https://doi.org/10.1016/j.jorganchem.2014.07.023.

[19] D. Xu, B. Cheng, S. Cao, J. Yu, Enhanced photocatalytic activity and stability of Z-scheme Ag2CrO4-GO composite photocatalysts for organic pollutant degradation, Appl. Catal. B Environ. 164 (2015) 380–388, https://doi.org/10.1016/j.apcatb.2014.09.051.

[20] D.W. Mayo, F.A. Miller, R.W. Hannah, Course Notes on the Interpretation of Infrared and Raman Spectra | Wiley https://www.wiley.com/en-mx/Course+Notes+on+the+Interpretation+of+Infrared+and+Raman+Spectra-p-9780471248231 (accessed 2020-11-17).

[21] M. Margoshes, V.A. Fassel, The infrared spectra of aromatic compounds: I. The out-of-plane C-H bending vibrations in the region 625–900 Cm−1, Spectrochim. Acta 7 (1955) 14–24, https://doi.org/10.1016/0371-1951(55)80003-3.

[22] W.R. Angus, C.R. Bailey, C.K. Ingold, C.L. Wilson, 211. Structure of benzene. Part I. The problem and experimental method, J. Chem. Soc. Resumed (1936) 912b–9915, https://doi.org/10.1039/JR936000912B.

[23] B.C. Smith, Infrared Spectral Interpretation: A Systematic Approach https://www.routledge.com/Infrared-Spectral-Interpretation-A-Systematic-Approach/Smith/p/book/9780849324635 (accessed 2020 -11 -17).

[24] I. Chakraborty, P. Baran, Y. Sanakis, A. Simopoulos, E. Fachini, R.G. Raptis, A mixed-valence octanuclear iron−oxo pyrazolate: assessment of electronic delocalization by structural and spectroscopic analysis, Inorg. Chem. 47 (24) (2008) 11734–11737, https://doi.org/10.1021/ic801459s.

[25] M. Sorai, IR spectra and spin equilibrium between the 6A1 and 2T2 states in Tris(N, N-diethyldithiocarbamato)iron(III), J. Inorg. Nucl. Chem. 40 (6) (1978) 1031–1034, https://doi.org/10.1016/0022-1902(78)80502-8.

[26] J. Blomquist, U. Helgeson, L.C. Moberg, B. Folkesson, R. Larsson, ESCA and Mössbauer spectra of some iron(III) betadiketonates and tetraphenylporphyrin iron (III) chloride, Inorganica Chim. Acta 69 (1983) 17–23, https://doi.org/10.1016/S0020-1693(00)83546-X.

[27] S. Srivastava, S. Badrinarayanan, A.J. Mukhedkar, X-ray photoelectron spectra of metal complexes of substituted 2,4-pentanediones, Polyhedron 4 (3) (1985) 409–414, https://doi.org/10.1016/S0277-5387(00)87000-X.

[28] C. Battistoni, A.M. Giuliani, E. Paparazzo, F. Tarli, Platinum complexes of the methyl esters of dithiocarbazic acid and 3-phenyldithiocarbazic acid, J. Chem. Soc. Dalton Trans. 7 (1984) 1293–1299, https://doi.org/10.1039/DT9840001293.

[29] M.M. Chehimi, M. Delamar, X-Ray Photoelectron Spectroscopy of Merocyanine Dyes: Part VII. Partial Charge and Conjugation of Heteroatoms in the Electrodonor Rings11For Preceding Papers in This Series, See Refs. (25–30). J. Electron Spectrosc. Relat. Phenom. 1989, 49 (2), 231. doi: 10.1016/0368-2048(89)85010-8.

[30] R.M. Silverstein, F.X. Webster, D.J. Kiemle, D.L. Bryce, Spectrometric Identification of Organic Compounds, 8th Edition | Wiley https://www.wiley.com/en-mx/Spectrometric+Identification+of+Organic+Compounds%2C+8th+Edition-p-9780470616376 (accessed 2020 -11 -17).

[31] C.J. Carrano, K.N. Raymond, Coordination chemistry of microbial iron transport compounds. 10. Characterization of the complexes of rhodotorulic acid, a dihydroxamate siderophore, J. Am. Chem. Soc. 100 (17) (1978) 5371–5374, https://doi.org/10.1021/ja00485a019.

[32] M. Roy, S. Saha, A.K. Patra, M. Nethaji, A.R. Chakravarty, Ternary iron(III) complex showing photocleavage of DNA in the photodynamic therapy window, Inorg. Chem. 46 (11) (2007) 4368–4370, https://doi.org/10.1021/ic062056l.

[33] W. Gawelda, A. Cannizzo, V.-T. Pham, F. van Mourik, C. Bressler, M. Chergui, Ultrafast nonadiabatic dynamics of [FeII(Bpy)3]2+ in solution, J. Am. Chem. Soc.

129 (26) (2007) 8199–8206, https://doi.org/10.1021/ja070454x10.1021/ja070454x.s001.
[34] R.M. El-Shazly, Synthesis and characterization of 3-methyl-5-oxo-N,1-diphenyl-4,5-dihydro-1-H-pyrazole-4-carbothioamide and its metal complexes, Spectrochim. Acta. A. Mol. Biomol. Spectrosc. 74 (1) (2009) 259–264, https://doi.org/10.1016/j.saa.2009.06.015.
[35] T. Duchanois, T. Etienne, C. Cebrián, L. Liu, A. Monari, M. Beley, X. Assfeld, S. Haacke, P.C. Gros, An iron-based photosensitizer with extended excited-state lifetime: photophysical and photovoltaic properties, Eur. J. Inorg. Chem. 2015 (14) (2015) 2469–2477, https://doi.org/10.1002/ejic.201500142.
[36] R. Nyquist, R. Kagel, Handbook of Infrared and Raman Spectra of Inorganic Compounds and Organic Salts - 1st Edition https://www.elsevier.com/books/handbook-of-infrared-and-raman-spectra-of-inorganic-compounds-and-organic-salts/nyquist/978-0-12-523450-4 (accessed 2020 -11 -17).
[37] E. Haro-Poniatowski, R. Rodríguez-Talavera, H.M. de la Cruz, O. Cano-Corona, R. Arroyo-Murillo, Crystallization of nanosized titania particles prepared by the sol-gel process, J. Mater. Res. 9 (8) (1994) 2102–2108, https://doi.org/10.1557/JMR.1994.2102.
[38] L. Liu, T. Duchanois, T. Etienne, A. Monari, M. Beley, X. Assfeld, S. Haacke, P. C. Gros, A new record excited state 3MLCT lifetime for metalorganic iron(II) complexes, Phys. Chem. Chem. Phys. 18 (18) (2016) 12550–12556, https://doi.org/10.1039/C6CP01418F.
[39] A. Kumar, P. Kumar, S. Paul, S.L. Jain, Visible light assisted reduction of nitrobenzenes using Fe(Bpy)3+2/RGO nanocomposite as photocatalyst, Appl. Surf. Sci. 386 (2016) 103–114, https://doi.org/10.1016/j.apsusc.2016.05.139.
[40] G. Lente, Deterministic Kinetics in Chemistry and Systems Biology: The Dynamics of Complex Reaction Networks; SpringerBriefs in Molecular Science; Springer International Publishing, 2015. doi: 10.1007/978-3-319-15482-4.
[41] C. Munikrishnappa, S. Kumar, S. Shivakumara, G. Mohan Rao, N. Munichandraiah, The TiO2-graphene oxide-hemin ternary hybrid composite material as an efficient heterogeneous catalyst for the degradation of organic contaminants, J. Sci. Adv. Mater. Devices 4 (1) (2019) 80–88, https://doi.org/10.1016/j.jsamd.2018.12.003.
[42] C.-K. Huang, T. Wu, C.-W. Huang, C.-Y. Lai, M.-Y. Wu, Y.-W. Lin, Enhanced photocatalytic performance of BiVO4 in aqueous AgNO3 solution under visible light irradiation, Appl. Surf. Sci. 399 (2017) 10–19, https://doi.org/10.1016/j.apsusc.2016.12.038.
[43] L. Xu, Y. Wei, W. Guo, Y. Guo, Y. Guo, One-pot solvothermal preparation and enhanced photocatalytic activity of metallic silver and graphene co-doped BiVO4 ternary systems, Appl. Surf. Sci. 332 (2015) 682–693, https://doi.org/10.1016/j.apsusc.2015.01.235.
[44] S.-Z. Wu, K. Li, W.-D. Zhang, On the heterostructured photocatalysts Ag3VO4/g-C3N4 with enhanced visible light photocatalytic activity, Appl. Surf. Sci. 324 (2015) 324–331, https://doi.org/10.1016/j.apsusc.2014.10.161.
[45] M. Pelaez, P. Falaras, V. Likodimos, K. O'Shea, A.A. de la Cruz, P.S.M. Dunlop, J. A. Byrne, D.D. Dionysiou, Use of selected scavengers for the determination of NF-TiO2 reactive oxygen species during the degradation of microcystin-LR under visible light irradiation, J. Mol. Catal. Chem. 425 (2016) 183–189, https://doi.org/10.1016/j.molcata.2016.09.035.
[46] J. Zhao, C. Chen, W. Ma, Photocatalytic degradation of organic pollutants under visible light irradiation, Top. Catal. 35 (3) (2005) 269–278, https://doi.org/10.1007/s11244-005-3834-0.
[47] A. Ajmal, I. Majeed, R.N. Malik, H. Idriss, M.A. Nadeem, Principles and mechanisms of photocatalytic dye degradation on TiO2 based photocatalysts: a comparative overview, RSC Adv. 4 (70) (2014) 37003–37026, https://doi.org/10.1039/C4RA06658H.